Vertical Drain and Overflow Pipes: Literature Review and New Experimental Data

R. Padulano, Ph.D.[1]; and G. Del Giudice, M.ASCE[2]

Abstract: This paper describes and discusses the available experimental investigations concerning vertical pipe flow in order to understand possible differences caused by different intake types and inflow conditions. Specific attention is given to the difference between drain pipes and overflow pipes and to the influence of the inflow conditions on the head–discharge relation. Data from the available literature are systematized and treated in a unified manner to provide a comprehensive view of possible flow regimes, among which four main types are selected, namely Borda free and full flow, governed by pipe cross section; weirlike flow, governed by pipe diameter; and full pipe flow, governed by pipe cross section and length. For each, both data from the literature and novel data are used to calibrate both dimensional and nondimensional head–discharge equations, along with prediction equations for the discharge coefficients. The equations describing the critical head, marking the passage to full pipe flow, and the vortex critical head, marking the passage to a vortex-free full pipe flow, are provided.
DOI: 10.1061/(ASCE)IR.1943-4774.0001311.

Author keywords: Borda free flow; Borda full flow; Critical head; Drain pipes; Full pipe flow; Head–discharge equation; Overflow pipes; Weirlike flow.

Introduction

Vertical drains consist of a vertical pipe whose intake is flush with the bottom of a tank; pipe diameter is usually small compared with the tank plan section, so that the flow approaches the pipe inlet from all directions. If the vertical pipe section is comparable with the tank section, a plunging flow occurs instead, following different dynamics, such as in drop manholes and plunging drop shafts (Camino et al. 2014; Granata et al. 2010). Vertical drains have different applications both in a residential context, such as roof rain leaders or tank drains (Kalinske 1940), and in large systems, such as drop shaft spillways of large dams, in which they are often followed by a culvert (Humphreys et al. 1970).

However, this topic has not received great attention in the literature, and only a few studies have performed experimental investigations (Kalinske 1940; Rahm 1953; Humphreys et al. 1970; Padulano et al. 2013, 2015; Banisoltan et al. 2016). Such experiments showed that flow mechanisms inside the drain are quite complex, involving different flow regimes and a large air entrainment causing an air–water mixture to flow along the system. As a consequence, vertical drains investigation gave rise to two different research segments: the head–discharge (h–Q) relation issue and the vortex formation issue.

The first issue was directly dealt with by Kalinske (1940), Humphreys et al. (1970), Banisoltan et al. (2016), Padulano et al. (2013, 2015), and Padulano and Del Giudice (2016), who conducted experiments addressing the different flow regimes, which usually coincide with different h–Q curves. Those authors observed similar flow regimes for extreme heads and discharges, whereas significant differences in the flow behavior were observed for intermediate values. When studying vertical drains, additional experimental data are usually taken into account involving different drop inlets such as the vertical overflow pipe, whose inlet section has a short but significant distance from the tank bottom (Binnie 1938; Kalinske 1940; Rahm 1953; Anwar 1965), and the bellmouth (Binnie 1938) or the morning glory intake (Wagner 1956; Fattor and Bacchiega 2001), because experimental evidence shows that those different intakes provide similar flow regimes. However, even when other experimental configurations were considered, only a general agreement about the equations describing the flow regimes was attained, but with significant differences both in the coefficient values of the h–Q equations and in the number of observed flow regimes. Finally, certain attention was given by the technical literature to a critical head marking the passage between two different flow regimes, or between two different branches of the h–Q relation (Kalinske 1940; Banisoltan et al. 2016).

Concerning the vortex issue, it is generally agreed that vertical pipes, regardless of the intake type, are affected by a severe air entrainment whose dynamics are highly dependent on the flow regime (Humphreys et al. 1970; Knauss 1987). For low heads and discharges, the flow usually enters the vertical pipe clinging to the pipe walls, leaving a central air core so that air enters directly into the pipe. For high heads and discharges, the pipe instead runs full and the air can only be entrained by means of occasional vortices that connect the free surface with the pipe intake. For intermediate heads and discharges, air entrainment is expected to occur as a combination of both, because the clinging jet experiences intermittent collapse, causing a periodical gulping of the central air core. For low/medium heads and discharges, several studies have measured air entrainment (Binnie 1938; Kalinske 1940), showing that air discharge flowing through the vertical pipe, starting from zero head, increases with increasing water discharge, reaching a maximum and then decreasing, approaching quasi-zero values immediately before switching to full pipe flow (FPF). After direct air entrainment ceases, air can still enter the pipe by means of

[1]Postdoctoral Researcher, Dept. of Civil, Architectural, and Environmental Engineering, Università degli Studi di Napoli Federico II, Naples, Italy (corresponding author). Email: roberta.padulano@unina.it

[2]Professor, Dept. of Civil, Architectural, and Environmental Engineering, Università degli Studi di Napoli Federico II, Naples, Italy. Email: delgiudi@unina.it

Note. This manuscript was submitted on April 10, 2017; approved on January 4, 2018; published online on April 12, 2018. Discussion period open until September 12, 2018; separate discussions must be submitted for individual papers. This paper is part of the ***Journal of Irrigation and Drainage Engineering***, © ASCE, ISSN 0733-9437.

completely developed vortices, which are vortices whose body protrudes inside the drop inlet (Knauss 1987). Several studies have investigated a vortex-related critical head marking the passage to an h–Q range in which no completely developed vortices can be observed and no air entrainment occurs (Kalinske 1940; Rahm 1953; Knauss 1987; Yildirim and Kocabas 1998).

This paper describes and discusses experimental investigations concerning vertical pipe flow in order to understand possible differences caused by different intake types and inflow conditions. Available data are systematized and treated in a unified manner to provide both dimensional and nondimensional equations for the main flow regimes, and to obtain equations describing the critical head, marking the passage to full pipe flow, and the vortex critical head, marking the passage to a vortex-free full pipe flow.

Experimental Campaigns Concerning Vertical Drains

Studies providing h–Q data for drain pipes, overflow pipes, or other intakes have observed different flow regimes within similar experimental ranges. This section analyzes available experimental campaigns in order to understand possible differences. Anderson et al. (1971) and Khatsuria (2005) also presented experimental observations, although their data are not strictly comparable to this research topic because of their particular experimental setups. Table 1 summarizes experiments; Fig. 1 shows related intake types. A preliminary evaluation shows that most of the experimental setups provide for a perfectly radial inflow in order to neglect the influence of the circulation in the tank [Fig. 2(a)] (Binnie 1938; Kalinske 1940; Anwar 1965; Banisoltan et al. 2016). Only the experiments performed by Rahm (1953), Humphreys et al. (1970), and Padulano et al. (2013, 2015) had a predominant approach flow direction and a supposedly significant circulation [Fig. 2(b)].

Data by Binnie (1938), available in a dimensional form, concerned a vertical overflow pipe with variable pipe length L and fixed diameter D, characterized by two different inlet crest shapes (A1 and A2 in Table 1) [Figs. 1(a and b)] and a radial inflow [Fig. 2(a)]. Starting from zero head, with increasing head and discharge (normal rising flow) the following flow regimes were observed: (1) an annular flow clinging to the pipe walls with a central air core [Fig. 3(a)]; (2) an annular flow with the central air core occasionally closing, causing instabilities in the free surface, with the frequency of choking increasing with increasing head; and (3) a flow regime with the pipe running full with occasional vortices [Fig. 3(b)]. For the shorter pipes, the so-called Borda free flow (BFR) spontaneously occurred: the nappe was detached from the pipe walls and the space between was filled with air, providing a significant increase in the water head in the tank [Fig. 3(c)]. In some experiments, when the head gained small values the nappe expanded to fill the pipe, called Borda full flow (BFL) [Fig. 3(d)] with a modification in the h–Q curve (BFR and BFL in Fig. 4). Data belonging to Regimes (1) and (2) lie on the same h–Q curve, in which any increase in Q causes only a small increase in h [weirlike flow (WF) in Fig. 4]. Data belonging to Regime (3) lie on a completely separate h–Q curve, so that any increase in Q causes a very large increase in h (FPF in Fig. 4). No attempt was made to provide an equation for the two curves; however, full pipe discharge is stated to be a function of $(h + L)^{0.5}$.

Kalinske (1940) provided nondimensional data of heads and discharges both for overflow and drain pipes (B1 and B2 in Table 1) [Figs. 1(b and c)] with variable D and L and a radial inflow [Fig. 2(a)] Two flow regimes were observed for increasing heads

Table 1. Summary of experimental campaigns concerning vertical pipes

		Tank			Pipe				
ID	Author	Shape	Dimensions $D_0/B \times b$	Approach flow	D (m)	L (m)	Code	Intake	Observations
A	Binnie (1938)	Cylindrical	1.3 m	Radial	0.027	0.6–1.5	A1	Overflow	Flat crest
							A2	Overflow	Sharp-edged crest
B	Kalinske (1940)	Cylindrical	1.8 m	Radial	0.044–0.148	1.2–5.2	B1	Overflow	Flat crest
							B2	Drain	
C	Rahm (1953)	Rectangular	6.5 m × 0.6 m	Unilateral	0.04–0.133	0.34–1.25	C1	Overflow	Flat crest, $t = 3.4$ mm, $D = 133$ mm
							C2	Overflow	Flat crest, $t = 1.6$ mm, $D = 83$ mm
							C3	Overflow	Flat crest, $t = 1.3$ mm, $D = 40$ mm
D	Anwar (1965)	Cylindrical	0.91 m	Radial	0.066–0.153	0.6	D11	Overflow	Rounded crest, $t = 9.7$ mm
							D12	Overflow	Rounded crest, $t = 9.2$ mm
							D13	Overflow	Rounded crest, $t = 6.5$ mm
							D14	Overflow	Rounded crest, $t = 5$ mm
							D21	Overflow	Flat crest, $t = 3.4$ mm
							D22	Overflow	Flat crest, $t = 1.6$ mm
							D23	Overflow	Flat crest, $t = 1.3$ mm
E	Humphreys et al. (1970)	Rectangular	2.743 m × 1.524 m	Unilateral	0.126	7.6[a]	E11	Overflow	Circulation eliminated
							E12	Overflow	Normally developed circulation
							E13	Overflow	Forced circulation
							E21	Drain	Circulation eliminated
							E22	Drain	Normally developed circulation
							E23	Drain	Forced circulation
F	Banisoltan et al. (2016)	Cylindrical	0.74 m	Radial	0.076	0.93	F1	Drain	$D_0 = 74$ cm
							F2	Drain	$D_0 = 61$ cm
							F3	Drain	$D_0 = 38$ cm
G	Novel data	Rectangular	1.03 m × 0.715 m	Unilateral	0.05–0.10	0.5–1.5	G1	Drain	$D = 10$ cm
							G2	Drain	$D = 7$ cm
							G3	Drain	$D = 5$ cm

[a]Length of vertical barrel.

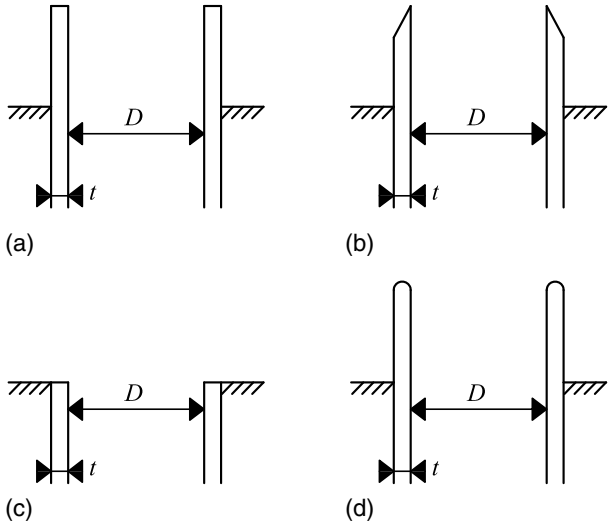

Fig. 1. Possible intake types: (a) flat crest (A1, B1, C1, C2, C3, D21, D22, D23, E11, E12, and E13); (b) sharp-edged crest (A2); (c) drain pipe (B2, E21, E22, E23, F1, F2, F3, G1, G2, and G3); and (d) rounded crest (D11, D12, D13, and D14).

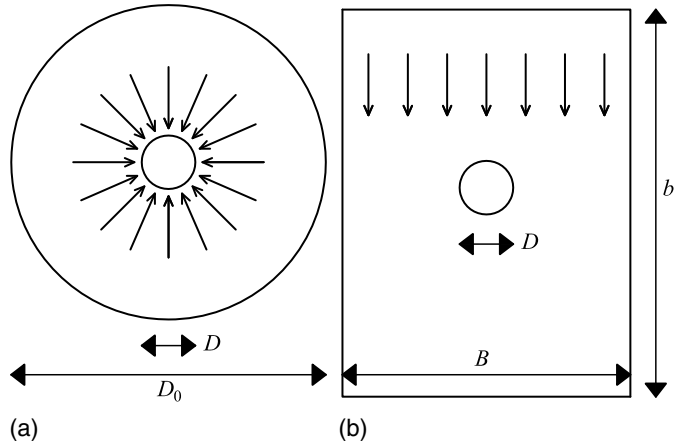

Fig. 2. Possible inflow conditions: (a) radial inflow; and (b) unilateral inflow.

and discharges: (1) a partially full pipe flow independent of the pipe length, in which the jet was annular, clinging to the pipe walls and with a central air core [Fig. 3(a)]; and (2) a full pipe flow with the pipe running completely full [Fig. 3(b)]. Air flow measurements proved that in partially full pipe flow the air discharge increased with h and Q, reached a maximum, and then decreased; in full pipe flow, air discharge was null but a small air entrainment was caused by some completely developed vortices [Fig. 3(b)] that occurred for the lowest heads of this flow regime. Experiments performed by Kalinske mainly focused on partially full pipe flow, so that only a few data were collected for full pipe flow. Table 2 lists the equations provided for the two flow regimes: for partially full pipe flow the equation was deduced empirically, whereas for full pipe flow it was obtained applying the energy principle. The intersection between the two equations gives the relative critical head h_{cr}/D, marking the passage between partially full and full pipe flow. Under some simplifying assumptions, h_{cr}/D was shown to be a function of L/D both for overflow and for drain pipes, although no empirical coefficients were provided. Finally, for partially full pipe flow the discharge coefficient was described as a complex function of h/D, whose equation was not given.

Rahm (1953) provided dimensional head–discharge data for an overflow pipe located at the end of a channel departing from a stilling tank [Fig. 2(b)]. The overflow pipe was placed at a distance of 0.9 m from the downstream wall of the channel and its intake section was placed at a distance of 0.6 m from the channel bottom to avoid any friction effect. Three different D and L combinations for the overflow pipe were observed (C1, C2, and C3 in Table 1); the pipe crest was always flat [Fig. 1(a)]. Four different flow regimes were observed: (1) a Borda free flow, with a central jet discharge with complete aeration around the jet, occurring from low to extremely high heads [Fig. 3(c)]; (2) a Borda full flow, namely a bottom orifice discharge with a central air core and clinging nappe [Fig. 3(d)], occurring for intermediate heads and causing a slight increase in discharge compared with Borda free flow (Fig. 4); (3) a weir flow, namely a weir-action discharge with clinging nappe and an intermittent aeration in the center of the pipe, often obstructed by accidental spray formation [Fig. 3(a)]; and (4) a full flow, with the pipe running full and occasional vortices with no influence on the head–discharge relation [Fig. 3(b)]. A spontaneous transition among the different flow types was observed for a fixed supply discharge, highlighting the possibility of unsteadiness in the water level above the intake. Table 2 lists the equations describing the different flow regimes. Moreover, additional experiments comparing radial inflow with the unilateral inflow (which was the object of the investigations) showed that the former did not exhibit any stable vortex occurrence, as opposed to the latter. However, no observations were made about a possible change in the head–discharge relation between the two cases.

Anwar (1965) provided nondimensional data of discharge coefficient for an overflow pipe with variable D and inlet crest thickness t and shape (D11–D23 in Table 1) [Figs. 1(a and d)] and a radial inflow [Fig. 2(a)]. The following flow regimes were observed: (1) a weir flow with an annular jet and central air core [Fig. 3(a)], whose discharge coefficient was an increasing function of h/D, depending on the wall thickness; (2) an orifice flow in which the pipe ran full [Fig. 3(b)], whose discharge coefficient was a function of t and crest shape but was constant with h/D; and (3) a Borda free flow [Fig. 3(c)] whose discharge coefficient was a complex function of h/D, also dependent on t and crest shape, reaching an asymptotic value for high h/D values. Table 2 lists the equations describing the different flow regimes.

Humphreys et al. (1970) performed experiments on a scale physical model of a closed-conduit spillway prototype with different inlet configurations, with the vertical pipe functioning both as an overflow (E11, E12, and E13 in Table 1) [Fig. 1(a)] and as a drain pipe (E21, E22, and E23 in Table 1) [Fig. 1(c)]. The test tank consisted of a stilling basin, a transition section, and a test section, so that there was a predominating flow direction [Fig. 2(b)] with no attempt to gain radial flow: this configuration is called normally developed circulation. Additional experiments were done both eliminating any circulation by means of a dike (no circulation) and increasing circulation by means of guide walls (forced circulation), in order to understand the effect of circulation on the h–Q relation. Moreover, vortex influence was studied by performing the same experiments both with and without an antivortex device. Experiments concerning normally developed circulation without any antivortex device showed the following different flow regimes for increasing heads and discharges: (1) a weir flow by drop inlet crest, in which the nappe could be either free [Fig. 3(e)] or clinging [Fig. 3(a)] (clinging nappe predominated except at very low heads), with a central air core; (2) a vortex flow, in which, for lower heads,

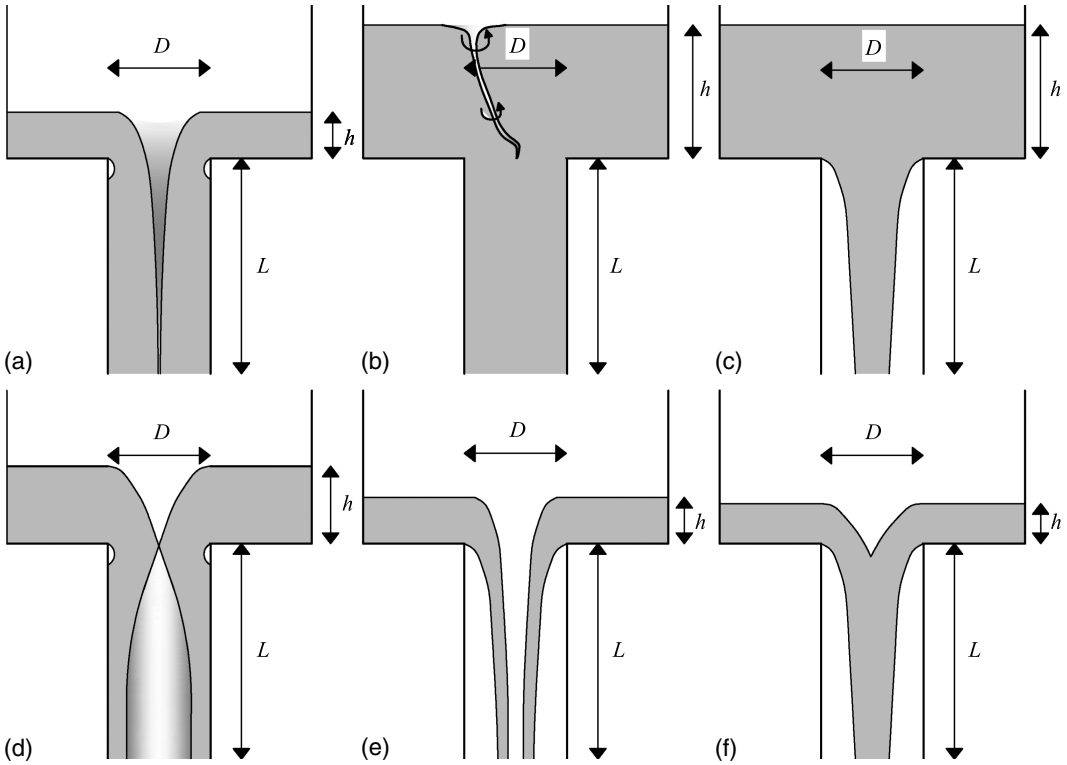

Fig. 3. Flow regimes: (a) weirlike flow; (b) full pipe flow; (c) Borda free flow with orifice control; (d) Borda full flow; (e) perfect weir flow; and (f) Borda free flow with weir control. Uniformly grey areas indicate water, white areas indicate air, and shading areas indicates air–water spray.

circulation only caused a twist in the weir flow nappe, whereas for higher heads the twist could unpredictably develop in a vortex, causing a rise in the water head; and (3) a full pipe flow for very high heads, with the pipe running full [Fig. 3(b)] and no vortices. For weir flow and full pipe flow, Table 2 lists the equations considered by Humphreys et al. (1970). The weir flow discharge coefficient was found to be an increasing function of h/D, with a different relation given for each of the experimental inlet configurations and circulation conditions. Concerning vortex flow, an envelope curve was proposed, whose intersection with full flow curves gives the critical head marking the passage to a vortex-free full flow region. Additional experiments showed that vortex flow cannot be observed when vortices are inhibited, although occasional vortices can be seen during both weir and full flow.

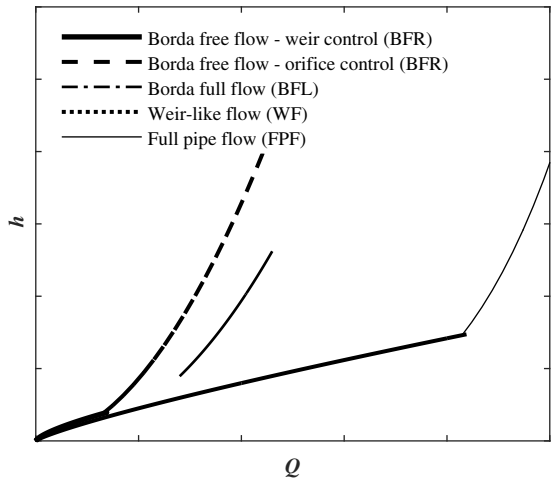

Fig. 4. Typical head–discharge for different flow regimes.

Furthermore, a comparison of forced and eliminated circulation showed that, for drain pipes, the water head above the inlet is higher for the former than for the latter condition.

Banisoltan et al. (2016) provided both dimensional and nondimensional h–Q data for a drain pipe with fixed D and L, with varying tank diameter D_0 (F1, F2, and F3 in Table 1) [Fig. 1(c)] and a radial inflow [Fig. 2(a)]. The following different flow regimes were observed: (1) for very low h and Q, a weir flow was observed with the nappe not touching the pipe walls and with a central air core [Fig. 3(e)]; (2) for slightly increasing h and Q, a weirlike flow was observed, with the nappe clinging to the inner pipe walls but still with a persisting central air core [Fig. 3(a)]; (3) on some occasions, a gulping caused the annular jet to change into a central jet, detaching from the pipe walls but with no central air core and a sudden increase in water head (orifice flow) [Fig. 3(c)]; (4) for increasing h and Q, a transitional flow was observed, in which a swirling air core with unstable diameter formed, causing instabilities in the free surface and with h being a function of Q^2; (5) for large h and Q, a full pipe flow was observed [Fig. 3(b)] with no significant vortex formation; and (6) the filling–emptying process, in which, starting from the weirlike regime, the flow spontaneously increased its head because of some circulation in the tank. The flow within the pipe coherently changed from an annular jet with a central air core to a less aerated flow. Once a maximum head was gained, flow changed back to weirlike flow. Table 2 lists the proposed equations for weirlike flow, full pipe flow, and orifice flow. Finally, drain pipe data collected by Kalinske (1940) were manipulated to fit the same equations, and the computed discharge coefficient C was used to calibrate the following equation:

$$C = 0.7\frac{h}{D} + 0.52 \tag{1}$$

showing that the weirlike discharge coefficient is a linearly increasing function of nondimensional water head.

Table 2. Flow regimes, proposed equations, and characteristic values

Author	Code	Available flow regimes	Proposed equations	K_e	C_{BFR}	C_{BFL}
Binnie (1938)	A1	WF[a], FPF[b], BFR[c], BFL[d]	—	0.55	0.58	0.70
	A2			1.01	0.51	0.63
Kalinske (1940)	B1	WF, FPF	WF: $Q = C \cdot h^2 \cdot \sqrt{gD}$	0.6[e]	—	—
	B2		FPF: $Q = C \cdot \pi/4 \cdot D^2 \cdot \sqrt{2g \cdot (h + L)}$ $C = (1 + K_e + f \cdot L/D)^{-0.5}$	0.7[e]	—	—
Rahm (1953)	C1	WF, FPF, BFR, BFL	WF: $Q = 2/3 \cdot 0.9 \cdot \pi D \cdot h \cdot \sqrt{2gh}$	0.72	0.56[e]	0.74
	C2		FPF: $Q = 0.7 \cdot \pi/4 \cdot D^2 \cdot \sqrt{2g \cdot (h + L)}$	0.93	0.57[e]	0.78
	C3		BFR: $Q = C \cdot \pi/4 \cdot D^2 \cdot \sqrt{2gh}$ BFL: $Q = C \cdot \sqrt{h}$	0.56	0.58[e]	0.71
Anwar (1965)	D11	WF, FPF, BFR	WF: $Q = C \cdot \pi D \cdot h \cdot \sqrt{2gh}$	0.39	0.67	—
	D12	WF, FPF, BFR	FPF: $Q = C \cdot \pi/4 \cdot D^2 \cdot \sqrt{2g \cdot (h + L)}$	—	0.67	—
	D13	FPF	BFR: $Q = C \cdot \pi/4 \cdot D^2 \cdot \sqrt{2gh}$	0.17	—	—
	D14	WF, FPF, BFR		0.31	0.66	—
	D21	BFR		—	0.56	—
	D22	FPF, BFR		—	0.57	—
	D23	FPF, BFR		—	0.57	—
Humphreys et al. (1970)	E11	WF, FPF, vortex flow	WF: $Q = C \cdot \pi D \cdot h^{1.5}$	0.56[e]/0.49[e]	—	—
	E12		FPF: $Q = C \cdot \pi/4 \cdot D^2 \cdot \sqrt{2g \cdot (h + L)}$	(with/without	—	—
	E13		$C = (1 + K_e + \Sigma K_i + \Sigma f \cdot L_i/D)^{-0.5f}$	antivortex	—	—
	E21			device)	—	—
	E22				—	—
	E23				—	—
Banisoltan et al. (2016)	F1	WF, FPF, BFR, transitional flow	WF: $Q = 2/3 \cdot C \cdot \pi D \cdot h \cdot \sqrt{2gh}$	0.1[e]	0.65[e]	—
	F2	WF, FPF, transitional flow, filling–emptying flow	FPF: $Q = C \cdot \pi/4 \cdot D^2 \cdot \sqrt{2g \cdot (h + L)}$	0.125[e]	—	—
	F3	WF, FPF, BFR, filling–emptying flow	$C = (1 + K_e + f \cdot L/D)^{-0.5}$ BFR: $Q = C \cdot \pi/4 \cdot D^2 \cdot \sqrt{2gh}$	0.15[e]	0.67[e]	—
Padulano et al. (2013, 2015) and novel data	G1	WF, FPF, BFR, transitional flow	WF: $Q = 2/3 \cdot C \cdot \pi D \cdot h \cdot \sqrt{2gh}$	0.2[e]	0.68	—
	G2		FPF: $Q = C \cdot \pi/4 \cdot D^2 \cdot \sqrt{2g \cdot (h + L)}$			
	G3		$C = (1 + K_e + f \cdot L/D)^{-0.5}$ BFR: $Q = C \cdot \pi/4 \cdot D^2 \cdot \sqrt{2gh}$			

[a]Weir flow regime (weir flow or partially full pipe flow).
[b]Full pipe flow regime (pressurized flow or orifice flow).
[c]Borda free flow regime (orifice flow).
[d]Borda full flow regime.
[e]Values from cited studies.
[f]Multiple local and friction head losses along pipe for Humphreys et al. (1970).

Experiments performed by Padulano et al. (2013, 2015) concerned a vertical drain with variable D and L (G1, G2, and G3 in Table 1) [Fig. 1(c)]. The flow approached the inlet with a predominating direction [Fig. 2(b)] passing from a detention tank to a filling tank through a filtering wall, which was the only device to reduce circulation, with no attempt to gain a perfectly radial inflow. For increasing heads and discharges the following flow regimes were observed: (1) a weir flow with the nappe clinging to the pipe walls and a central air core with frequent gulping [Fig. 3(a)]; (2) a transitional flow with the water head oscillating between a maximum and a minimum for each experienced discharge; and (3) a pressurized flow with the pipe running full [Fig. 3(b)]. Padulano et al. (2013, 2015) presented only a qualitative description of the flow regimes because their main focus was the effects of a peculiar venting system. Only for pressurized flow was an equation provided for the drain pipe condition (Table 2) along with an estimate for the entrance loss coefficient.

Novel Experiments

The experimental model consisted of a rectangular tank with a $0.7 \times 2.07 \times 1.25$ m^3 volume. The flow approached the intake section of the drain pipe with a predominating direction [Fig. 2(b)], passing from a detention tank to a filling tank through a filtering wall. The vertical drain pipe was centrally attached to the bottom of the filling tank [Fig. 1(c)]. Three different D for the drain pipe were used (10, 7, and 5 cm) in combination with three different L (1.5, 1, and 0.5 m). Supply discharge entered the detention tank vertically downward from a supply line, whose outlet section, parallel to the tank bottom, was placed at about half the height of the tank. As a consequence, when the water head in the tank was high, the supply outlet section was submerged; for lower water heads, the supply discharge impinged against the tank bottom, creating an extremely turbulent motion pattern, which could be only partially dissipated by the filtering wall. This setup was intended to simulate a hydraulic plant with a unilateral inflow (more realistic than radial inflow) and without any device aimed at reducing turbulence or circulation.

Experiments were performed by varying the discharge flowing through the system and measuring the water head which settled in the tank; point gauges were adopted for flow depth measurement, with an accuracy of $\pm 0{:}5$ mm, whereas an orifice-plate differential-pressure flowmeter was used for discharge measurements, with an accuracy of ± 1 L/s. Both an emptying and a filling path were followed in order to verify whether any hysteretic behavior occurred,

with no significant results. In accordance with the findings by Padulano et al. (2013, 2015), the observed flow regimes were a weir flow regime [Fig. 3(a)], transitional flow, and pressurized flow [Fig. 3(b)]. Concerning the transitional flow, data corresponding to the minimum water heads were added to the weir flow data set, significantly increasing the number of data for this flow regime. Finally, Borda free flow was observed when the pipe length was reduced to 1, 2, and 3 times the pipe diameter.

Head–Discharge Relation

This section provides a comprehensive description of the main flow regimes observed in two or more studies. Equations are provided in both dimensional and nondimensional forms and different intake types are compared, if possible. The flow regimes of interest are (1) Borda free flow; (2) Borda full flow; (3) weirlike flow; and (4) full pipe flow (Fig. 3). In accordance with literature, the following nondimensional parameters were used: the nondimensional water head h/D, the pipe Froude number $\mathrm{F}_D = Q \cdot (gD^5)^{-0.5}$ (Hager and Del Giudice 1998), and the nondimensional pipe length L/D.

Borda Free Flow

Borda free flow (also known as orifice flow) consists of a falling jet detaching from the inlet crest of the vertical pipe, with the external surface subject to atmospheric pressure [Fig. 3(c)]; in this flow regime the jet never touches the inner pipe walls. This implies, theoretically, that such a flow is not possible for long pipes ($L \gg D$), which do not grant adequate aerating conditions (Kalinske 1940); however, experiments by Binnie (1938) exhibited Borda free flow for L/D ratios up to 24.

According to the cited literature, for Borda free flow the h–Q relation can be expressed by the following equation:

$$Q = C_{\mathrm{BFR}} \cdot \frac{\pi D^2}{4} \cdot \sqrt{2gh} \tag{2a}$$

or, in a nondimensional form

$$\mathrm{F}_D = C_{\mathrm{BFR}} \cdot \frac{\pi\sqrt{2}}{4} \cdot \sqrt{\frac{h}{D}} \tag{2b}$$

In Eq. (2), the pipe length L does not appear as a governing variable, consistent with the assumption that pipe walls do not interact with the falling jet in any way. Therefore it is expected that the classical discharge coefficient for pure bottom orifice flow (namely with $L = 0$) occurs; such a value is usually set equal to 0.610 (Lienhard and Lienhard 1984). However, C_{BFR} in Eq. (2) was found to be significantly different. This is because C_{BFR}, like the discharge coefficient for pure bottom orifice flow, is very sensitive to any minor malformation of the orifice and has a dependence on the inflow Reynolds number (Lienhard and Lienhard 1984). This implies that a certain dependence on the water head should be expected. Moreover, it is possible that pipe length hinders a perfect aeration of the jet, causing an additional change in C_{BFR}.

Fig. 5 shows C_{BFR} computed for each experimental point by inverting Eq. (2), as a function of h/D for overflow pipe data [Fig. 5(a)] and for drain pipe data [Fig. 5(b)]. Two different behaviors are evident: starting from a minimum h/D, C_{BFR} increases,

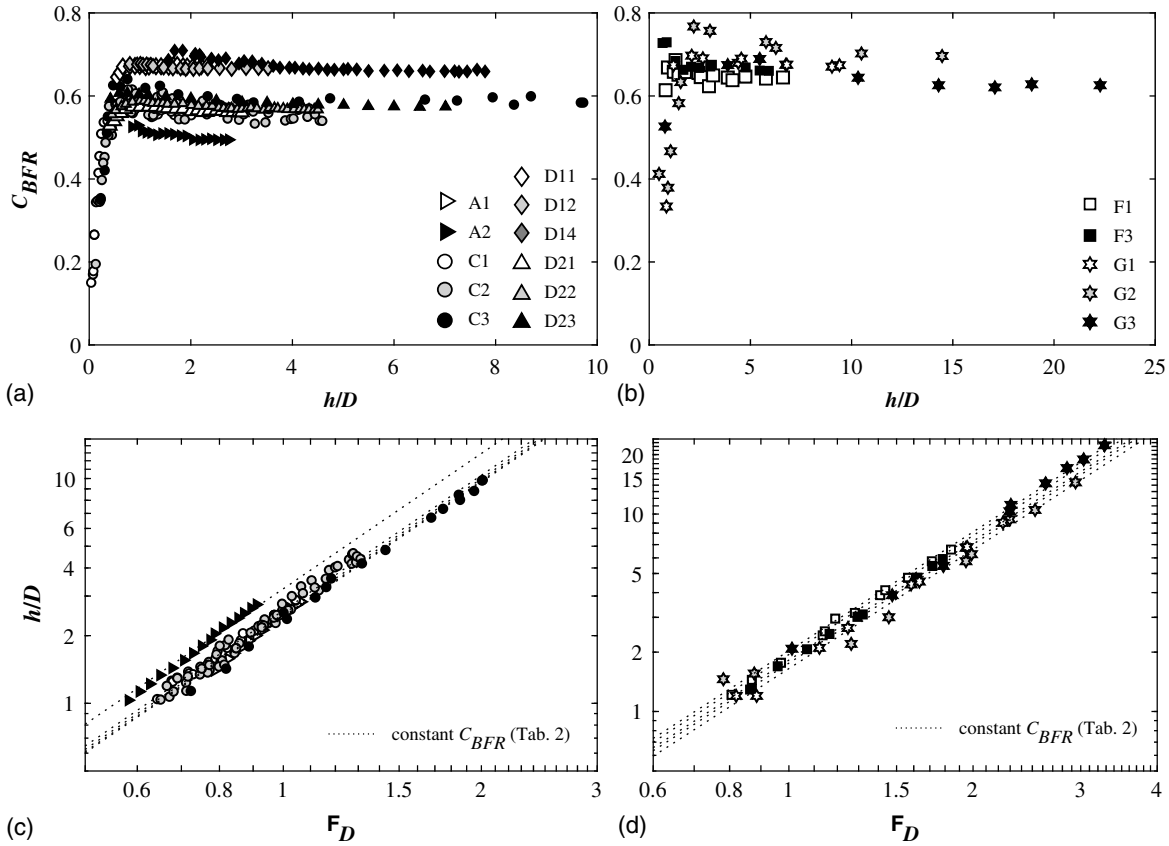

Fig. 5. Available BFR nondimensional data: (a–c) discharge coefficients and head–discharge relation for overflow pipes; and (b–d) for drain pipes.

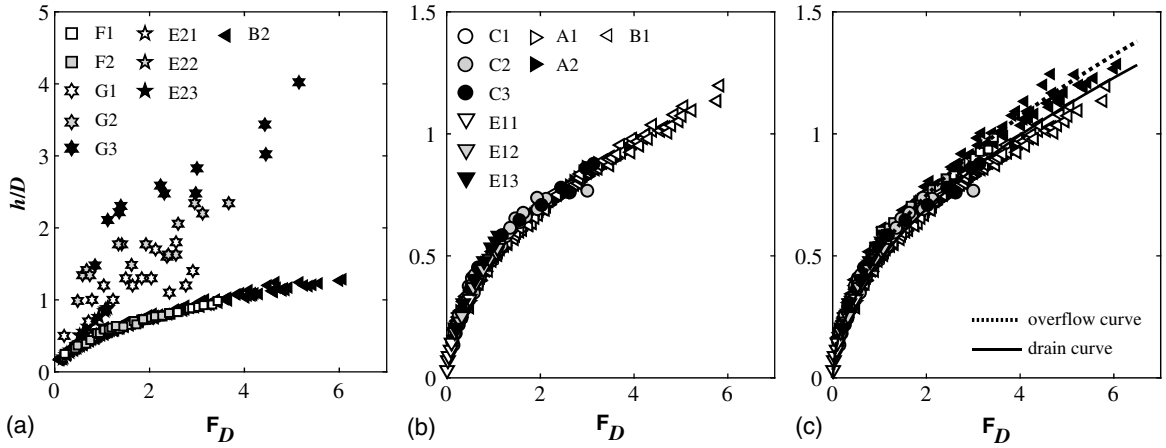

Fig. 6. Weirlike flow nondimensional head–discharge relation: (a) for drain pipes; (b) for overflow pipes; and (c) for WFn conditions.

reaches a maximum and decreases to an asymptotical value, which, for overflow pipes, decreases moving from rounded to flat to sharp-edged pipe wall crests. This can be explained by the fact that, for very small nondimensional water heads, a funnel-shaped inflow cavity forms, with the apex of this conical cavity plunged inside the pipe intake [Fig. 3(f)]. This cavity is inactive with respect to flow and causes the discharge to be controlled by the weir above the edge of the pipe (Rahm 1953). For increasing water head, the cavity becomes shallower and moves farther from the intake section, causing the transition to bottom orifice control, and finally disappears for high values of h/D [Fig. 3(c)]. This also causes the passage from the first to the second branch of the Borda free flow h–Q relation (BFR in Fig. 4). Rahm (1953) provided a threshold of $h/D = 0.3$ for the transition from weir control to orifice control. However, experimental evidence shows that the threshold should be higher to contain all the data in Figs. 5(a and b); the present paper suggests a threshold of $h/D = 1$ for both overflow and drain pipe data.

Once Borda free flow with orifice control is gained, the discharge coefficient slightly decrease with increasing h/D. However, Figs. 5(c and d) show that if a constant value of C_{BFR} is considered in Eq. (2), the evaluation of Q and F_D is highly satisfying nonetheless. Table 2 gives the constant C_{BFR} reported by the cited studies, or newly computed when needed.

Borda Full Flow

According to the description by Binnie (1938) and Rahm (1953), during Borda full flow, an air core develops from the water surface to the pipe intake section; below the intake section, the air core expands, filling a great part of the cross section of the pipe, with the water flowing in a thin annular jet clinging to the pipe walls [Fig. 3(d)]. The h–Q relation is similar to that of Borda free flow with orifice control in Eq. (2), but higher discharge coefficients C_{BFL} were experienced (Table 2). A possible dependence on the pipe length was expected because the falling nappe adheres to the pipe walls, but was not found.

For each data set exhibiting Borda full flow (A1, A2, C1, C2, and C3), the ratio $(C_{\mathrm{BFL}} - C_{\mathrm{BFR}})/C_{\mathrm{BFR}}$ was computed, describing the increase in the discharge coefficient passing from Borda free flow to Borda full flow, with an average value of 0.34. This implies that, during Borda full flow, the discharge flowing through the pipe is 34% greater than during Borda free flow, on average.

Weirlike Flow

A perfect weir flow is usually characterized by a falling nappe which is subject to atmospheric pressure on the free surface; as a consequence, the nappe is expected to have a perfectly aerated central air core and the space between the external surface with the inner pipe walls filled with air [Fig. 3(e)]. However, this perfectly aerated condition is almost impossible to achieve, both because the pipe length does not allow air to recirculate and because the central air core is usually sealed with spray when the head over the intake increases [Fig. 3(a)]. In this case, the cited literature showed that the h–Q relation is still governed by the intake diameter (or perimeter); this is why this peculiar flow regime was defined as weirlike flow, although the usual discharge coefficients for weir flow cannot be expected. The equation governing weirlike flow is

$$Q = \frac{2}{3} \cdot C_{\mathrm{WF}} \cdot \pi D \cdot h \cdot \sqrt{2gh} \tag{3a}$$

or, in a nondimensional form

$$\mathsf{F}_D = C_{\mathrm{WF}} \cdot \frac{2\sqrt{2}}{3} \cdot \pi \cdot \left(\frac{h}{D}\right)^{\frac{3}{2}} \tag{3b}$$

All data in the cited literature were rearranged to fit Eq. (3) and they were used to compute C_{WF}. Fig. 6(a) shows that when drain pipe points are compared, two distinct clusters form, the first gathering the greater part of available data and the second consisting of the E23, G1, G2, and G3 data sets. The E23 data points related to an experimental condition characterized by a forced circulation in the plant by means of peculiar devices, whereas the G1–G3 data points related to an experimental condition in which no attempt was made to reduce the extremely highly turbulent and complex motion pattern of water in the plant. The remaining data sets (B2, E21, E22, F1, and F3) related to experimental conditions in which either the inflow to the vertical drain was perfectly radial (B2, F1, and F3), or the inflow was unilateral but devices were used to reduce circulation (E21). The E22 data set exhibited the same behavior as E21 even though no anticirculation devices were used. This could be due to the fact that the stilling chamber, upstream of the approach channel, was efficient in dissipating circulation and in straightening the motion pattern, as opposed to in the E23 and G1–G3 data sets. The remainder of this paper divides weirlike flow into weirlike flow with no significant circulation (WFn) and weirlike flow with

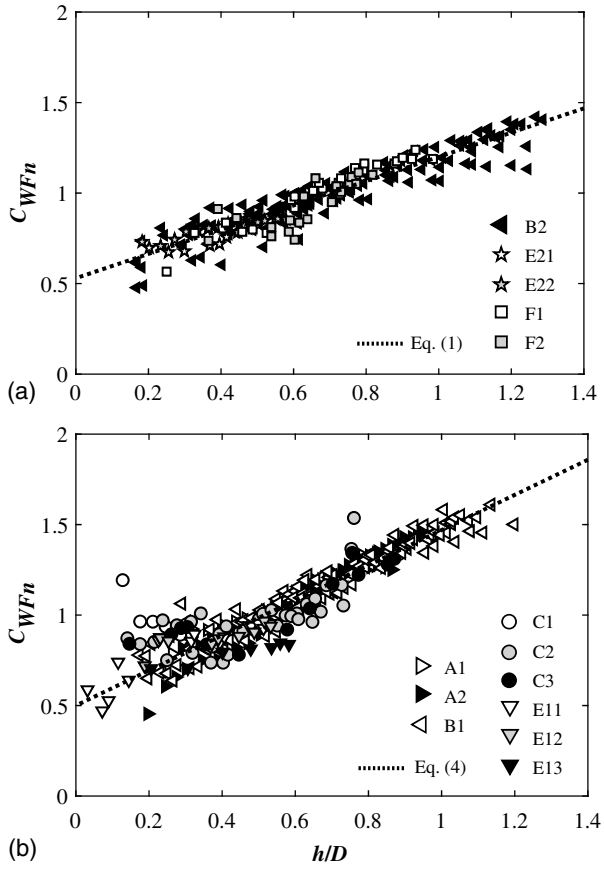

Fig. 7. WFn discharge coefficient as a function of nondimensional water head for (a) drain pipes; and (b) overflow pipes.

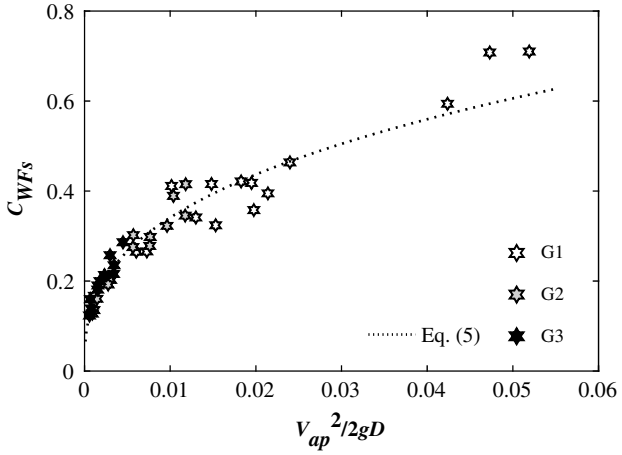

Fig. 8. Weirlike flow discharge coefficient as a function of nondimensional velocity head under WFs conditions.

significant circulation (WFs). It is evident from Fig. 6(a) that WFn and WFs follow different head–discharge laws, so that discharge is higher for WFn than for WFs for a fixed head. Furthermore, the G1, G2, and G3 data were significantly scattered, suggesting the existence of multiple h–Q relations.

Fig. 6(b) shows h–Q nondimensional data for overflow pipes. Once again, the involved data sets concerned both data with radial inflow and/or anticirculation devices (A1, A2, B1, and E11), and data with forced or not prevented circulation (C1, C2, C3, E12, and E13). In this case, however, all the experimental points seem to follow the same h–Q law. Such a difference cannot be justified at present, because of the differences in the experimental setups and in the covered h–Q range.

Fig. 6(c) compares WFn data both for drain and for overflow pipes, showing that the drain pipe intake decreased the hydraulic capacity of the pipe, causing a reduction of the pipe Froude number with respect to overflow pipes for a fixed nondimensional water head.

When circulation was negligible (WFn condition), the discharge coefficient C_{WFn} had a linearly increasing dependence on h/D (Fig. 7). For overflow pipes, the interpolation of data provides

$$C_{\mathrm{WFn}} = 0.91 \cdot \frac{h}{D} + 0.54 \tag{4}$$

with $R^2 = 87\%$, whereas drain pipe data are interpolated by Eq. (1) (Banisoltan et al. 2016). In both cases, the relationship between discharge coefficient and nondimensional water head was linear. However, Fig. 6(c) shows that, if C_{WFn} is considered a constant, the overall dependence of F_D on h/D is quadratic [$\mathsf{F}_D = \alpha \cdot (h/D)^2$], with R^2 equal to 99 and 96% for drain pipes and overflow pipes respectively, and α equal to 3.6 and 4.3, respectively.

When circulation is significant (WFs), the correlation between the discharge coefficient C_{WFs} and h/D is unsatisfying, so that other dependences must be sought. Circulation is caused by a predominating approach velocity component, which causes the flow to impinge against the opposite tank wall and to create a twist in the falling jet; consequently, this velocity component V_{ap} (and the corresponding nondimensional velocity head $V_{ap}^2/2gD$) can be adopted as a measure of circulation. Fig. 8 shows that C_{WFs}, computed by inverting Eq. (4) for novel data, is a function of $V_{ap}^2/2gD$ by means of the following equation, with $R^2 = 90\%$:

$$C_{\mathrm{WFs}} = 1.77 \cdot \left(\frac{V_{ap}^2}{2gD}\right)^{0.36} \tag{5}$$

where $V_{ap} = Q/(hB)$, where B = tank width [Fig. 2(b)]; however, it is possible to rearrange nondimensional velocity head as a combination of all the previously defined nondimensional parameters to make its computation more straightforward. If the approach Froude number is defined as $\mathsf{F}_{ap} = V_{ap}/\sqrt{gh}$, the continuity principle implies that the discharge flowing through the pipe equals the discharge approaching the vertical pipe, which gives the relationship between the pipe and the approach Froude numbers

$$\mathsf{F}_{ap} \cdot Bh \cdot \sqrt{gh} = \mathsf{F}_D \cdot \sqrt{gD^5} \Rightarrow \mathsf{F}_{in} = \mathsf{F}_D \cdot \frac{D}{B} \cdot \left(\frac{h}{D}\right)^{-(3/2)} \tag{6}$$

Thus, the following expression for the approach nondimensional velocity head can be obtained:

$$\frac{V_{in}^2}{2gD} = \frac{1}{2} \cdot \mathsf{F}_D^2 \left(\frac{D}{B}\right)^2 \cdot \left(\frac{h}{D}\right)^{-2} \tag{7}$$

Substituting Eq. (7) into Eq. (5) leads to the evaluation of the WFs discharge coefficient as a function of pipe Froude number, nondimensional water head, and the ratio D/B.

If the C_{WFs} estimated in this manner is used in Eq. (3), it is possible to evaluate the h–Q relation for novel data (Fig. 9). As a consequence, this relation proves to be parametrized by the ratio D/B because the G1, G2, and G3 data have the same tank width but different pipe diameters. Fig. 9 also shows that the increase in the

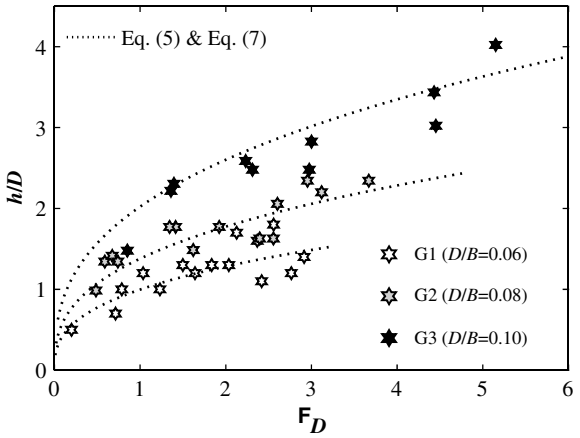

Fig. 9. Nondimensional head–discharge points and equations for novel data.

water head provided by circulation increases for decreasing D/B, namely for small pipe diameters and large tanks.

Full Pipe Flow

This flow regime is characterized by the pipe running full with no visible air entrainment apart from sporadic vortices [Fig. 3(b)], which do not cause any change in the hydraulic capacity of the pipe. All the cited studies agreed about the equation describing the h–Q curve, which stems from the application of the energy principle between the intake section and the outflow section

$$Q = C_{\mathrm{FPF}} \cdot \frac{\pi}{4} D^2 \cdot \sqrt{2g \cdot (h + L)} \tag{8a}$$

or, in a nondimensional form

$$\mathrm{F}_D = C_{\mathrm{FPF}} \cdot \frac{\pi\sqrt{2}}{4} \cdot \sqrt{\frac{h}{D} + \frac{L}{D}} \tag{8b}$$

FPF is the only case in which the discharge coefficient has an analytical expression, namely

$$C_{\mathrm{FPF}} = \sqrt{\frac{1}{1 + K_e + f \cdot L/D}} \tag{9}$$

where K_e = entrance loss coefficient. The Darcy–Weisbach friction factor f is a function of relative roughness (all the available experimental campaigns involved smooth pipes) and Reynolds number, which is a function of pipe velocity, and consequently of h and Q. However, C_{FPF} can be considered substantially constant with h/D (Fig. 10) and only dependent on the pipe material, nondimensional length, and entrance loss coefficient. Table 2 lists the estimated values of the entrance loss coefficient for the aforementioned experimental campaigns; it is quite evident that K_e is very sensitive to the experimental conditions because no generalization can be made.

Critical Heads

This section analyzes novel data to obtain information about nondimensional critical head h_{cr}/D, marking the passage to FPF, and nondimensional vortex critical head h_v/D, marking the passage to a vortex-free FPF region. For both, a correlation is sought with significant nondimensional parameters, and some equations are provided and compared with existing literature.

Critical Head

If each different h–Q curve is described by an equation, the intersection of pairs of equations gives the head and discharge marking the passage from one flow regime to another. Specifically, it is of utmost importance to predict the passage to full pipe flow, because this is the flow regime showing the greatest increase in the water head. If the transition point is underestimated, the vertical pipe could suffer an unexpected reduction in its hydraulic capacity, leading to a rapid surge in the water head and a possible surcharge in the upstream system with consequent backwater effects. However, although the FPF equation has widespread consensus in the literature, it is not straightforward to decide which other equation to consider as the intersecting curve. In Binnie (1938), Kalinske (1940), and Rahm (1953) FPF was directly preceded by WF. In Humphreys et al. (1970), FPF was preceded by WF if some anti-vortex device was adopted, or by a vortex flow if vortices were not prevented. In Padulano et al. (2013) and Padulano and Del Giudice (2016), FPF was preceded by a transitional flow with the head oscillating between a maximum and a minimum for each discharge. In Banisoltan et al. (2016), FPF was preceded by WF in some cases and by a transitional flow with $h = f(Q^2)$ in other cases. Each cited work stated that when the passage to FPF is approached, the free surface suffers a certain instability, which hinders precise water head measurements that can be compared with any theoretical results.

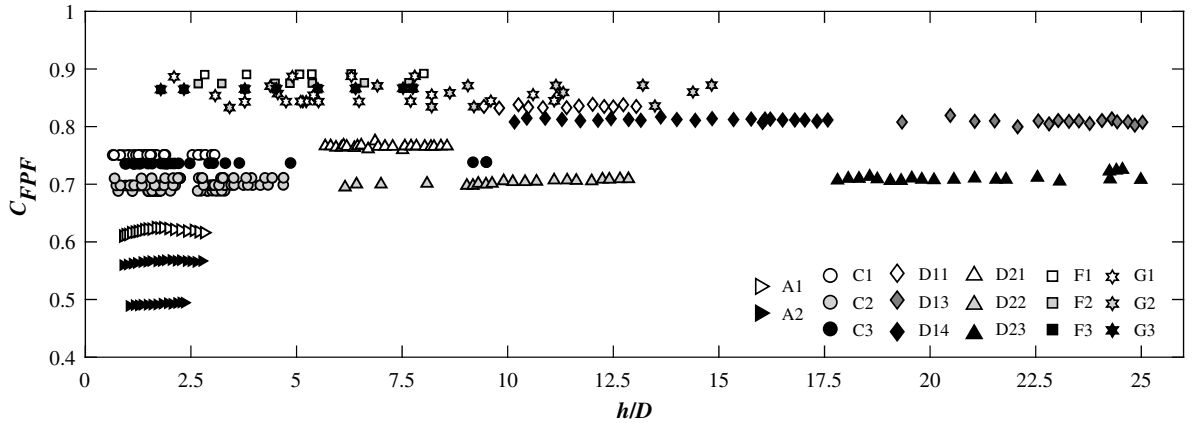

Fig. 10. Full pipe flow discharge coefficient as a function of nondimensional water head.

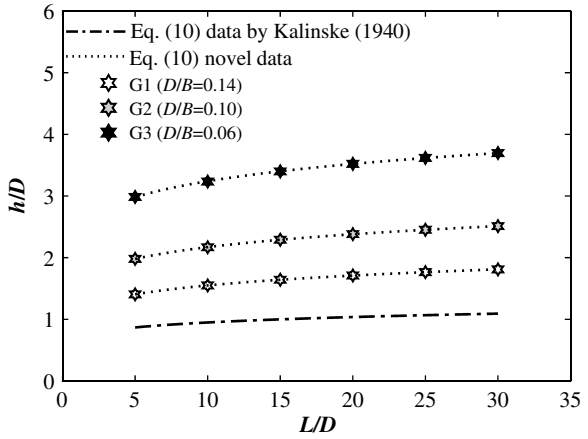

Fig. 11. Relation between nondimensional critical water head and nondimensional length.

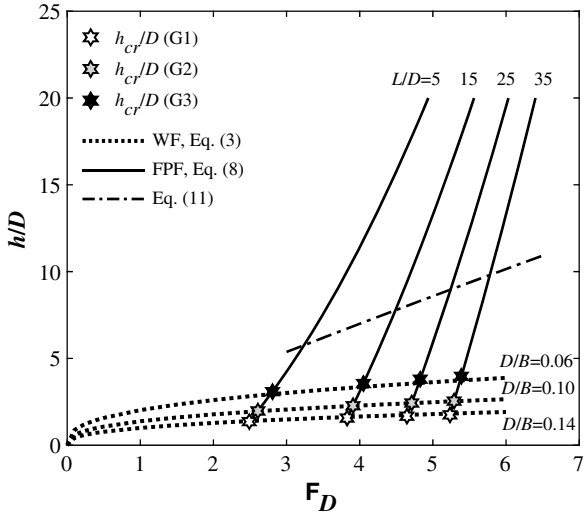

Fig. 12. Theoretical curves describing WF, FPF, and vortex critical head for novel data.

Whatever h–Q equations are used to intersect, h_{cr} will depend on the same parameters. Therefore, if the non-dimensional WF and FPF curves are considered, h_{cr}/D will inherit from WF a dependence on circulation (as shown in previous sections, the h–Q equation is unique when circulation is negligible, whereas it is parametrized by the ratio D/B for significant approach flow velocity) and from FPF a dependence on friction factor (namely on the pipe roughness), on the entrance head loss (namely on the intake type) and, most of all, on L/D (whose variations determine a change in h_{cr}/D even if all the other variables are fixed). For novel data, the flow regime preceding FPF was described as a transitional flow with oscillating water head (Padulano et al. 2013, 2015). However, it was observed that the amplitude of oscillations decreased to zero when approaching the passage to FPF, so that no significant distortion was made in the prediction of h_{cr}/D if the WF curve [Eq. (3)] was intersected with the FPF curve [Eq. (8)]. The computed h_{cr}/D can be successfully correlated to the nondimensional pipe length (Fig. 11)

$$\frac{h_{cr}}{D} = \beta \cdot \left(\frac{L}{D}\right)^{0.13} \tag{10}$$

where $\beta = 1.1$, 1.6, and 2.5 for G1 to G3 data, respectively, in other words, for decreasing D/B.

Fig. 11 also shows the curve derived by Kalinske (1940) and confirmed by Banisoltan et al. (2016), computed using Eq. (10) with $\beta = 0.7$. As expected, there was a less-than-linearly increasing dependence on L/D; the main difference lay in the presence of circulation which causes a considerable increase in h_{cr}/D. To validate Eq. (10), h_{cr}/D was verified to be higher than the highest nondimensional WFs h/D and lower than the lowest nondimensional FPF h/D for each L/D.

Vortex Critical Head

During the experimental campaign described by Padulano et al. (2013, 2015) and Padulano and Del Giudice (2016), vortices were observed within several flow regimes; in all cases, vortex formation was promoted by the asymmetrical direction of flow (Durgin and Hecker 1978). Several types of vortex were observed depending on the flow regime; particularly for FPF, the only form of air entrainment was the completely developed air core vortex, corresponding to Vortex Type 6 (VT6) in the Alden Research Laboratory classification (Knauss 1987) [Fig. 3(b)]. VT6 vortices were especially observed when large diameters and lengths were adopted, because of the high depression values at the shaft intake; they were usually followed by an impulsive increase in depression values, associated with a prolonged gurgling noise and vibrations in the shaft. Furthermore, if a persistent and large vortex occurred, causing an abrupt pressure reduction, a slight increase in the water head was seen because of a sudden reduction in the shaft effective section, which was partially occupied by the vortex itself. However, these occurrences were rare and the full flow regime was sufficiently stable for a long time, providing significant measurements of water head.

Advanced methods to predict vortex critical head involve some significant nondimensional parameters such as the circulation number, and some characteristic dimensions of the vortex shape (Knauss 1987). However, computation of these parameters requires specific measurements which are rarely available; in this case, an often-used method (Humphreys et al. 1970; Gordon 1970; Jain et al. 1978) is to evaluate vortex critical head by relating it to the intake Froude number by means of a power function, whose exponent is expected to be equal or lower than 1 when circulation is weak and about 2 when circulation is strong. Of course, such an equation is strongly related to the geometrical configuration of the investigated intake system and may not be generalized. For novel data, a similar power function was evaluated by enveloping the lowest FPF water heads in which no vortices were seen during the tests

$$\frac{h_v}{D} = 1.96 \cdot \mathrm{F}_D^{0.92} \tag{11}$$

that represents the head–discharge line separating vortex-free full flow region from the full flow region in which vortices are possible. Fig. 12 shows WF and FPF curves, expressed by Eqs. (3) and (8) with parameter values corresponding to the G1, G2, and G3 tests, along with the equation describing vortex critical head, Eq. (11). Fig. 12 shows that the vortex critical head is always higher than critical head in the experimental range, implying that vortices should always be expected in FPF.

Conclusions

This paper reviewed the literature concerning vertical drain and overflow pipes with the intake types shown in Fig. 1. Specifically, available experimental data were organized and investigated to provide a comprehensive classification of possible flow regimes and the corresponding head–discharge relations. Four main flow regimes were observed, namely (1) a weirlike flow, governed by the pipe diameter, consisting of an annular jet with a frequently choking air core and occurring at low heads and discharges; (2) a full pipe flow, governed by the pipe cross section and length, in which the pipe runs full with no significant air entrainment, occurring at high heads and discharges; (3) a Borda free flow, governed by the pipe cross section, consisting of a falling nappe whose envelope surface is under atmospheric pressure; and (4) a Borda full flow, occurring at intermediate h and Q and causing an increase in discharge compared with Borda free flow.

For BFR, BFL, WF, and FPF, the equations for the h–Q curves were calibrated in both a dimensional and a nondimensional form using available experimental data [Eqs. (2), (3), and (8), respectively], and the discharge coefficients were analyzed to look for possible dependences on significant experimental parameters. Comparisons of drain pipes and overflow pipes were performed when possible. Particular attention was paid to WF, for which novel data were considered along with literature tests; for this flow regime, the data analysis showed a strong influence of circulation on the discharge coefficient. Specifically, when circulation is negligible, the discharge coefficient can be successfully predicted by means of the nondimensional water head only; in contrast, the discharge coefficient can be related to the pipe Froude number, the nondimensional water head, and the ratio of the pipe diameter to the tank width.

Finally, novel data were used to calibrate the equations predicting the critical head, marking the passage to FPF, and the vortex critical head, marking the passage to the FPF vortex-free region [Eqs. (10) and (11), respectively]. The former was found to be dependent only on the pipe nondimensional length, whereas the latter was found to be dependent on the pipe Froude number; both findings were in accordance with the existing literature.

Notation

The following symbols are used in this paper:

B = tank width (L);
b = tank length (L);
C = discharge coefficient in the h–Q equation;
D = pipe diameter (L);
D_0 = tank diameter (L);
F_{ap} = approach Froude number;
F_D = pipe Froude number;
f = Darcy–Weisbach friction factor;
h = water head (L);
h_{cr} = critical head (L);
h_v = vortex critical head (L);
K_e = entrance loss coefficient;
L = pipe length (L);
Q = discharge ($L^3 \cdot T^{-1}$);
V_{ap} = approach velocity ($L \cdot T^{-1}$);
α = empirical coefficient for weirlike flow quadratic equation; and
β = empirical coefficient for critical head equation.

Subscripts

BFR = Borda free flow;
BFL = Borda full flow;
FPF = full pipe flow;
WFn = weirlike flow with negligible circulation; and
WFs = weirlike flow with significant circulation.

References

Anderson, A. G., P. Vaidyaraman, and C. Chu. 1971. *Hydraulics of long vertical conduits and associated cavitation*. Project Rep. No 122. Minneapolis: Univ. of Minnesota.

Anwar, H. O. 1965. "Coefficients of discharge for gravity flow into vertical pipes." *J. Hydraul. Res.* 3 (1): 1–19. https://doi.org/10.1080/00221686509500076.

Banisoltan, S., N. Rajaratnam, and D. Z. Zhu. 2016. "Experimental and theoretical investigation of vertical drains with radial inflow." *J. Hydraul. Eng.* 143 (5): 04016103. https://doi.org/10.1061/(ASCE)HY.1943-7900.0001277.

Binnie, A. M. 1938. "The use of a vertical pipe as an overflow for a large tank." *Proc. R. Soc. London, Ser. A, Math. Phys. Sci.* 168 (933): 219–237. https://doi.org/10.1098/rspa.1938.0171.

Camino, G. A., N. Rajaratnam, and D. Z. Zhu. 2014. "Choking conditions inside plunging dropshafts." *Can. J. Civ. Eng.* 41 (7): 624–632. https://doi.org/10.1139/cjce-2014-0033.

Durgin, W. W., and G. E. Hecker. 1978. "The modelling of vortices at intake structures." In Vol. 1 of *Proc., IAHR-ASME-ASCE Joint Symp. on Design and Operation of Fluid Machinery*, 381–391. Fort Collins, CO: CSU.

Fattor, C. A., and J. D. Bacchiega. 2001. "Analysis of instabilities in the change of regime in morning-glory spillways." In Vol. 29 of *Proc. XXIX IAHR Congress*, 656–662. Bejing.

Gordon, J. L. 1970. "Vortices at intakes." *J. Water Power* 22 (4): 137–138.

Granata, F., G. De Marinis, and R. Gargano. 2010. "Hydraulics of circular drop manholes." *J. Irrig. Drain. Eng.* 137 (2): 102–111. https://doi.org/10.1061/(ASCE)IR.1943-4774.0000279.

Hager, W. H., and G. Del Giudice. 1998. "Generalized culvert design diagram." *J. Irrig. Drain. Eng.* 124 (5): 271–274. https://doi.org/10.1061/(ASCE)0733-9437(1998)124:5(271).

Humphreys, H. W., G. Sigurdsson, and H. J. Owen. 1970. *Model test results of circular, square and rectangular forms of drop-inlet entrance to closed-conduit spillways*. Rep. of Investigation No. 65. Champaign, IL: Illinois State Water Survey.

Jain, A. K., K. G. Ranga Raju, and R. J. Garde. 1978. "Vortex formation at vertical pipe intakes." *J. Hydraul. Div.* 104: HY10.

Kalinske, A. A. 1940. *Hydraulics of vertical drain and overflow pipes*. Iowa City, IA: Iowa Institute of Hydraulic Research.

Khatsuria, R. M. 2005. *Hydraulics of spillways and energy dissipators: Civil and Environmental Engineering Series*. New York: Marcel Dekker.

Knauss, J., ed. 1987. *Swirling flow problems at intakes*. Rotterdam, Netherlands: A.A.Balkema.

Lienhard, J. H., and J. H. Lienhard. 1984. "Velocity coefficients for free jets from sharp-edged orifices." *J. Fluids Eng.* 106 (1): 13–17. https://doi.org/10.1115/1.3242391.

Padulano, R., and G. Del Giudice. 2016. "Transitional and weir flow in a vented drop shaft with a sharp-edged intake." *J. Irrig. Drain. Eng.* 142 (5): 06016002. https://doi.org/10.1061/(ASCE)IR.1943-4774.0001011.

Padulano, R., G. Del Giudice, and A. Carravetta. 2013. "Experimental analysis of a vertical drop shaft." *Water* 5 (4): 1380–1392. https://doi.org/10.3390/w5031380.

Padulano, R., G. Del Giudice, and A. Carravetta. 2015. "Flow regimes in a vertical drop shaft with a sharp-edged intake." *J. Appl. Water Eng. Res.* 3 (1): 29–34. https://doi.org/10.1080/23249676.2015.1026417.

Rahm, L. 1953. "Flow of water discharged through a vertical over flow pipe." In Vol. 71 of *Flow Problems with Respect to Intakes and Tunnels*

of Swedish Hydro-electric Power Plants, 71–117. Stockholm, Sweden: Royal Institute of Technology.

Rajaratnam, N., A. Mainali, and C. Y. Hsung. 1997. "Observations on flow in vertical dropshafts in urban drainage systems." *J. Environ. Eng.* 123 (5): 486–491. https://doi.org/10.1061/(ASCE)0733-9372(1997)123:5(486).

Wagner, D. L. 1956. "Morning-glory shaft spillways, a symposium: Determination of pressure-controlled profiles." *Trans. Am. Soc. Civ. Eng.* 121 (1): 345–368.

Yildirim, N., and F. Kocabas. 1998. "Critical submergence for intakes in still-water reservoirs." *J. Hydraul. Eng.* 124 (1): 103–104. https://doi.org/10.1061/(ASCE)0733-9429(1998)124:1(103).